

Quantum interference and spin polarization on Rashba double quantum dots

Kuo-Wei Chen and Ching-Ray Chang

Department of Physics, National Taiwan University, Taipei 10617, Taiwan

Abstract

We report on the quantum interference and spin accumulation on double quantum dots with Rashba spin-orbit coupling and electron-electron interaction, based on the Keldysh nonequilibrium Green function formalism. It is shown that Rashba spin-orbit interaction can strongly affect the conductance spectrum. By gradually increasing the Rashba parameter from zero, Fano resonances in strong overlap regime continuously evolve to resolve antiresonances. This transition is ascribed to the phase shift of couplings between molecular states and the lead due to spin precession. We also show that both bias and Rashba effect strengthen the induced spin polarization in this device. For particular energy position, up- and down-spin electron occupation can intersect to form a crossing point. Spin polarization on different side of this point has opposite sign in consequence. The magnitude and direction of spin polarization are therefore controllable by tuning the dot levels and the Rashba parameter through gates.

I. INTRODUCTION

Spin-related phenomena in semiconductor nanostructures are important subjects and of fundamental interest in condensed matter physics and material science.¹ In particular, studying the spin-orbit interaction, combined with applied external fields, to manipulate the electron spin and to generate the spin-polarized current in spintronic devices is strongly desired.² Among different structures a great deal of experimental and theoretical researches had been reported on quantum transport properties through quantum dot (QD) systems due to potential applications, from spintronic devices to quantum information.³ Control of the spin states of electrons confined in QDs is the challenges to build these spin-based devices.

Mechanisms inducing spin-orbit coupling in QD systems, including both structure and bulk inversion asymmetries, have been recently studied,^{4,5} in the hope that spin states of electrons can be coherently controlled.^{6,7,8} Among these two mechanisms the Rashba spin-orbit (RSO) coupling is of more potential applicability, because of its coupling strength tunability via the interface electric field controllable by either applied gate voltage or doping.⁹ A built-in asymmetric potential underlying Rashba mechanism causes a moving electron to precess about the effective magnetic field. Throughout the transport a precession angle of an electron spin is thus generated. Quantum interference consequent on the electron spins with different precession angles is modulated by tunable RSO coupling strength, as expected.

A variety of coupled QDs structures with sizes smaller than electron coherence length have been achieved in mesoscopic solid-state circuits.¹⁰ The important characteristics of preserved coherence of electrons in QD systems, such as the Aharonov-Bohm oscillation^{11,12} and the Fano effect^{13,14,15}, have been widely observed. The latter arises from the interference between a discrete state and the continuum.¹⁶ For coupled double QDs (DQD), an interdot coupling brings coherent hopping through tunneling barrier between two dots, which causes the level repulsion of DQD and meanwhile complicates the electron transport through the system.¹⁷ On the way to understand the electron transport considering RSO interaction, the dephasing and interference can be studied via the Fano effect, which had been proved to be an effective method.¹⁸ On the other hand the behavior of spins in dots each and the relation in between, corresponding to tunable RSO effect, are also required.

In this paper we study the quantum transport through a ring with serially coupled DQD. Quantum interference arises from the electron waves passing through different paths under

the influence of the RSO interaction. For electrons in one lead, the ways across the system to the other contain a bridge channel and four molecular states separated by the interdot coupling and the electron-electron interaction. Concerning the system out of equilibrium associated with a finite bias, the spin-dependent conductance is calculated based on the Keldysh Green function formalism.¹⁹ We show that the RSO interaction strongly affects the resonances in conductance both in weak and strong bias condition. When varying the Rashba parameter, the phases of tunneling couplings between molecular states and the lead are gradually changed, accompanied with the formations of Fano antiresonances. We also study the spin accumulation phenomenon on DQD. Above the Kondo temperature the dots are unpolarized without external magnetic field, while spin-polarized occupation is shown to exist in this device due to the combined effect of a bridge channel and the RSO coupling. Advantageously the spin polarization (SP) is sensitive to the level position and the Rashba coupling strength on dots. The manipulation of the SP, such as magnitude and direction, can therefore be easily achieved by tuning gate voltage, which may be useful in the design of spintronic devices.

The paper is organized as follows. In Sec. II we describe the model and the self-consistent procedure used to obtain the nonequilibrium Green functions in current expression. In Sec. III we show the interference phenomena both in weak and strong bias condition. Differential conductance is discussed in three cases of different controlling ways of the energy levels on two dots. In Sec. IV we show the spin accumulation induced in this device and study the behavior of SP as the bias and the RSO coupling are varied. Then final conclusions are gathered in Sec. V.

II. THE MODEL

The device is illustrated in Fig. 1, where the ring-dot structure is realized on the heterostructure confining a two-dimensional electron gas (2DEG). In semiconductor the energy separation between single-electron levels has been reported to be a considerable energy scale due to the small effective mass. Therefore, only single energy level near the Fermi surface is assumed to be relevant in each dot. Two dots, with both RSO coupling and Coulomb interaction taken into account, are connected in series and embedded in one arm of the ring, and then attached to two normal metal leads. No interaction exists on the bridge channel.

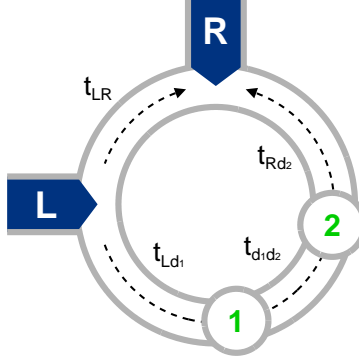


FIG. 1: (Color online) Double quantum dots coupled serially to leads, denoted as L and R, with Rashba spin-orbit coupling and on-site Coulomb repulsion.

Experimentally one can tune the electron density on the dot and the couplings to the leads by using several gates.²⁰

We begin with the following model Hamiltonian

$$H = H_0 + H_B + H_D + H_T, \quad (1)$$

where the terms

$$H_0 = \sum_{\alpha\mathbf{k}\sigma} \epsilon_{\alpha\mathbf{k}} n_{\alpha\mathbf{k}\sigma} + \sum_{i\sigma} (\epsilon_i n_{i\sigma} + U n_{i\uparrow} n_{i\downarrow}), \quad (2)$$

$$H_B = \sum_{\mathbf{k}\mathbf{k}'\sigma} t_{LR} \left(a_{L\mathbf{k}\sigma}^\dagger a_{R\mathbf{k}'\sigma} + a_{R\mathbf{k}'\sigma}^\dagger a_{L\mathbf{k}\sigma} \right), \quad (3)$$

$$H_D = \sum_{\sigma} t_{d_1 d_2} \left(d_{1\sigma}^\dagger d_{2\sigma} + d_{2\sigma}^\dagger d_{1\sigma} \right), \quad (4)$$

and

$$H_T = \sum_{\mathbf{k}\sigma} t_{Ld_1} a_{L\mathbf{k}\sigma}^\dagger d_{1\sigma} + t_{Rd_2} e^{-i\sigma\varphi} a_{R\mathbf{k}\sigma}^\dagger d_{2\sigma} + H.c. \quad (5)$$

are explained below. The number operators for the corresponding states of the dot spin and the lead spin are given by $n_{i\sigma} = d_{i\sigma}^\dagger d_{i\sigma}$ and $n_{\alpha\mathbf{k}\sigma} = a_{\alpha\mathbf{k}\sigma}^\dagger a_{\alpha\mathbf{k}\sigma}$, respectively, where the fermionic operator $d_{i\sigma}$ ($d_{i\sigma}^\dagger$) destroys (creates) an electron with spin $\sigma = \uparrow, \downarrow$ on the i th ($i = 1, 2$) dot, and $a_{\alpha\mathbf{k}\sigma}$ ($a_{\alpha\mathbf{k}\sigma}^\dagger$) destroys (creates) an electron with energy $\epsilon_{\alpha\mathbf{k}}$ in the lead $\alpha = L, R$.

The first term in H_0 describes the leads, which are modeled by Fermi sea with energy $\epsilon_{\alpha\mathbf{k}}$. Each lead is filled up to an electrochemical potential μ_α , and the occupation number obeys the Fermi distribution $f_\alpha(\omega) = \{\exp[(\omega - \mu_\alpha)/k_B T] + 1\}^{-1}$. The second and third terms

in H_0 correspond to the isolated dots. Each dot consists of a single level ϵ_i and an on-site Coulomb repulsion with constant strength U . Note that the dot levels are assumed to be spin degenerate since the effect of the RSO coupling simply contributes to an extra phase in the tunneling matrix elements, when choosing a space-dependent spin coordinate.²¹ The terms H_B and H_D account for the bridge channel between two leads with coupling strength t_{LR} and the hopping between two dots with coupling strength $t_{d_1 d_2}$, respectively. The last term H_T is the couplings of the dots to the leads. For simplicity we have assumed all the tunneling matrix elements to be spin-independent. Owing to the RSO coupling there is a spin-dependent phase $\varphi = \alpha_R m^* L / \hbar^2$ generated in the path through the dots, with α_R being the Rashba parameter and L being the size of the DQD.

Applying the same procedure introduced in Ref. 21, we now analyze the quantum transport property of this device through the Keldysh nonequilibrium Green function technique. The charge current flowing from the left lead into the ring can be calculated from the time evolution of the occupation number for electrons in the left lead, which is written as²²

$$I_\sigma = \frac{2e}{\hbar} \int \frac{d\omega}{2\pi} \text{Re} [t_{Ld_1} G_{d_1 L \sigma}^<(\omega) + t_{LR} G_{RL \sigma}^<(\omega)], \quad (6)$$

where the lesser Green function $G_{ij \sigma}^<(\omega)$ correlates the states in i and j with spin σ . The spin-dependent conductance is thus defined as $G_\sigma = dI_\sigma/dV$. From the kinetic equation and the assumption of ideal leads, the lesser Green functions are related to the retarded and advanced Green functions through

$$G_\sigma^< = G_\sigma^r g_\sigma^{r-1} g_\sigma^< g_\sigma^{a-1} G_\sigma^a. \quad (7)$$

In order to obtain the lesser Green functions, the retarded Green functions are calculated by the Dyson equation

$$G_\sigma^r = g_\sigma^r + g_\sigma^r \Sigma_\sigma^r G_\sigma^r, \quad (8)$$

where the retarded Green function G_σ^r in the local basis is a 4×4 matrix

$$G_\sigma^r \equiv \begin{bmatrix} G_{LL\sigma}^r & G_{LR\sigma}^r & G_{Ld_1\sigma}^r & G_{Ld_2\sigma}^r \\ G_{RL\sigma}^r & G_{RR\sigma}^r & G_{Rd_1\sigma}^r & G_{Rd_2\sigma}^r \\ G_{d_1L\sigma}^r & G_{d_1R\sigma}^r & G_{d_1d_1\sigma}^r & G_{d_1d_2\sigma}^r \\ G_{d_2L\sigma}^r & G_{d_2R\sigma}^r & G_{d_2d_1\sigma}^r & G_{d_2d_2\sigma}^r \end{bmatrix}. \quad (9)$$

The bare Green functions g_α^r in the leads with wide-band approximation are taken in the form $g_\alpha^r = -i\pi\rho$, and $g_{d_i d_i \sigma}^r$ on the dots can be obtained exactly by the equation of motion

method

$$g_{d_i d_i \sigma}^r(\omega) = \frac{\omega - \epsilon_i - U + U n_{i-\sigma}}{(\omega - \epsilon_i)(\omega - \epsilon_i - U)}, \quad (10)$$

where ρ is the density of states of the leads and $n_{i-\sigma}$ is the occupation number with spin $-\sigma$ on the i th dot. The self-energy neglecting higher-order terms is written as the tunneling matrix

$$\Sigma_\sigma^r(\omega) \equiv \begin{bmatrix} 0 & t_{LR} & t_{Ld_1} & 0 \\ t_{LR}^* & 0 & 0 & \tilde{t}_{Rd_2} \\ t_{Ld_1}^* & 0 & 0 & t_{d_1 d_2} \\ 0 & \tilde{t}_{Rd_2}^* & t_{d_1 d_2}^* & 0 \end{bmatrix}, \quad (11)$$

with $\tilde{t}_{Rd_2} = t_{Rd_2} e^{-i\sigma\varphi}$. This approximation is sufficient above the Kondo temperature to study the Fano resonance and spin accumulation. The occupation number in Eq. (10) is determined self-consistently by the equation

$$n_{i\sigma} = -i \int \frac{d\omega}{2\pi} G_{d_i d_i \sigma}^<(\omega). \quad (12)$$

III. DIFFERENTIAL CONDUCTANCE

In numerical calculation we set $\rho = 1$, and all the tunneling matrix elements are simplified as constants $t_{LR} = 0.1$, $t_{Ld_1} = t_{Rd_2} = 0.4$, and $t_{d_1 d_2} = 0.8$. The temperature is set to $k_B T = 0.0001$ ($T \approx 1.16$ K). The Fermi level is here set as the origin of energy, and the energies are in units of $\Gamma \equiv 2\pi\rho t_{\alpha d_i}^2 \approx 1$. A symmetric bias V applied to two leads results in a chemical potential difference so that $\mu_L = -\mu_R = V/2$. We have determined a distinguishing point in the plot of differential conductance versus bias voltage, as shown later in Fig. 5(a). The value of bias at this point is about $V = 0.2$ which equals ten percent of Coulomb repulsion strength $U = 2$. Below this value differential conductance differs from zero bias conductance within one percent and is basically considered as a constant. Above this value differential conductance departs from the constant and noticeably changes with both bias and RSO coupling strength. Therefore, we discuss the system defined in weak and strong bias conditions by regions below and above $V = 0.2$, respectively.

A. Weak bias

Excluding the cases with level position on dot well below and above the equilibrium chemical potential, an electron in lead with weak bias potential can hardly overcome the Coulomb energy to fill an occupied state. The interference is thus expected to arise mainly from the mixing of electron waves through a molecular state and the bridge channel.

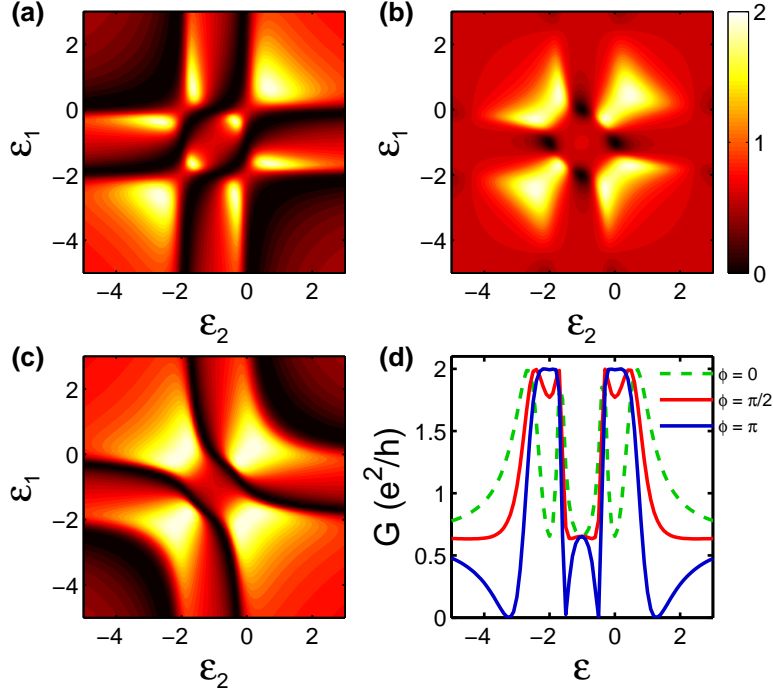


FIG. 2: (Color online) Conductance spectrum with weak bias $V = 0.02$ at (a) $\varphi = 0$, (b) $\varphi = \pi/2$, and (c) $\varphi = \pi$. (d) Differential conductance with $\epsilon_1 = \epsilon_2 \equiv \epsilon$ for $\varphi = 0, \pi/2, \pi$.

Figures 2(a)–(c) show the whole conductance spectrum as a function of individual dot levels ϵ_1 and ϵ_2 for three RSO coupling strength $\varphi = \alpha_R m^* L / \hbar^2 = 0, \pi/2, \pi$. We can clearly observe that the total conductance is strongly affected by the RSO coupling, including the phases and the positions of the resonances and antiresonances, which we then discuss. Consider the case $\epsilon_1 = \epsilon_2 \equiv \epsilon$, as shown in Fig. 2(d). In the absence of RSO coupling two Coulomb peaks are located at $\epsilon = 0$ and $\epsilon = -U$. The single-particle energy ϵ is modified by the interdot coupling and the tunneling couplings of the dots to the leads. Each Coulomb peak thus split into two peaks associated with the bonding and antibonding states. Without bridge channel the electron transport is described by two pairs of Breit-Wigner resonances,

with a Coulomb gap in between, at the energies of molecular states and unaffected by the RSO interaction. In present configuration, a change in the phase difference between bonding and antibonding resonances is here observed, when the RSO coupling is varied. Electrons passing through two different pathways result in the quantum interference, which is characterized by the Fano resonance corresponding to an asymmetric line shape in the conductance curve. The Fano effect at $\varphi = 0$ in Fig. 2(d) is modified since no antiresonance is found in the conductance. This disappearance of antiresonances is ascribed to the strong overlap within each pair of Fano resonances due to the large interdot coupling, which results in the mergence of antiresonances.¹⁷ As φ increases, four antiresonances occur at $\varphi = \pi$ as a consequence of destructive quantum interference, and the value of the conductance remains the same at $\epsilon = -1$. During the spin precession on dots, a spin-dependent phase shift takes place in dot-lead matrix elements $t_{Rd_2}e^{-i\sigma\varphi}$. From $\varphi = 0$ to $\varphi = \pi$ the phase parameter s of dot-lead matrix element is altered from $s = +1$ to $s = -1$ in the complex plane for both up- and down-spin electrons,²³ which leads to a phase evolution of electron transport through four molecular states. Each pair of Fano resonances at $\varphi = \pi$ is thus still out of phase within.²⁴ Moreover, one can see that the RSO effect on the interference is present to offset the suppression of the Fano antiresonances, because the typical Fano line shape is completely restored.

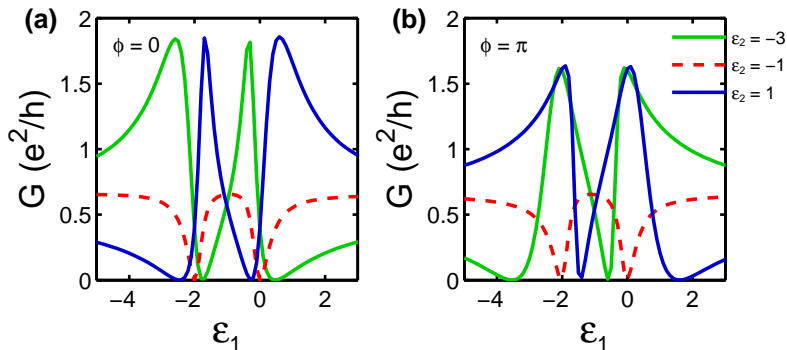


FIG. 3: (Color online) Differential conductance for $\epsilon_2 = -3, -1, 1$ at (a) $\varphi = 0$ and (b) $\varphi = \pi$.

We now address the electron transport through a tunable level, while the other is fixed at particular energy position. Hence the conductance versus the dot level ϵ_1 is plotted at three values of $\epsilon_2 = -3, -1, 1$ under the RSO interaction. In Fig. 3(a), with $\varphi = 0$, the conductance shows the typical two-level Fano line shapes. The Fano parameter is

continuously altered by different values of ϵ_2 from the left side to the right side of $\epsilon_2 = -1$, corresponding to negative value through zero to positive value. In Fig. 3(b), with $\varphi = \pi$, the conductance still shows the Fano line shapes. However, the Fano parameters change sign except the curve at $\epsilon_2 = -1$, in comparison with the corresponding curves in Fig. 3(a). We note that in conformity with all molecular states varied by the RSO coupling, as shown in Fig. 2(d), the phases of two resonances are here simultaneously changed from the observation on the same sign of Fano parameters.

B. Strong bias

In addition to the coherent transport, a strong bias shifts the energies of the electrons in two leads. The nonequilibrium situation, with a bias voltage $\mu_L = -\mu_R = 2$ across the ring-dot system, is built up and contributes to the electrical current through the device. With this increase of the bias window excited states become accessible and participate in the transmission. Meanwhile, the charge fluctuation can occur, and the interference between molecular states is enlarged. The mixture of various interference among bridge channel and molecular states thus complicates the transport through the device.

Figures 4(a)–(c) show the whole conductance spectrum as a function of individual dot levels ϵ_1 and ϵ_2 for three RSO coupling strength $\varphi = 0, \pi/2, \pi$. We can clearly observe that the total conductance here is still affected by the RSO coupling and is very different from that in the weak bias condition. Consider the case $\epsilon_1 = \epsilon_2 \equiv \epsilon$, as shown in Fig. 4(d). In the absence of RSO coupling there are eight peaks in the conductance curve. These peaks are distinctly located around $\epsilon = -4, -2, 0, 2$. In each pair of peaks the energy separation is associated with the interdot coupling and the tunneling couplings of the dots to the leads. The doubled peaks are ascribed to the electron conduction when each molecular state is aligned with either of leads. One can see that the maximum values of these peaks are lower than those in the weak bias condition. With increasing φ the splits within pairs of peaks decrease and the antiresonances in between form. This transition is the same as that in Fig. 2(d) due to the s -dependence of couplings to the lead, except for the suppressed Fano antiresonances at $\varphi = \pi$. The change in Fano line shapes indicates that the phase of the electron transmitting via both bonding and antibonding states is shifted with difference π by the RSO coupling. In addition, the value of conductance at $\epsilon = -1$, unlike weak bias,

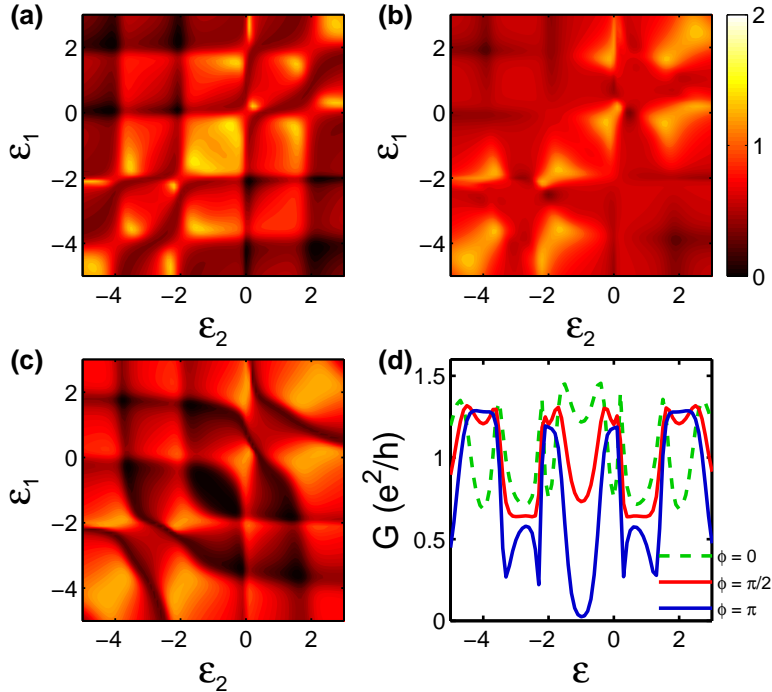


FIG. 4: (Color online) Conductance spectrum with strong bias $V = 4$ at (a) $\varphi = 0$, (b) $\varphi = \pi/2$, and (c) $\varphi = \pi$. (d) Differential conductance with $\epsilon_1 = \epsilon_2 \equiv \epsilon$ for $\varphi = 0, \pi/2, \pi$.

does not remain the same. We thus study further the behavior of the conductance at this point, as shown in Fig. 5(a). In weak bias condition, $V < 0.1U$, the conductance is almost unaffected by the RSO coupling. However, the conductance with different values of RSO coupling strength can be enhanced to two or be reduced to zero at certain values of larger bias voltage.

Consider now the situation with a fixed level $\epsilon_2 = -3, -1, 1$. Figures 5(b)–(d) show the conductance as a function of the dot level ϵ_1 for $\varphi = 0, \pi/2, \pi$. At $\varphi = 0$, as shown in Fig. 5(b), the sign change of the Fano parameter, symmetric with respect to the curve at $\epsilon_2 = -1$ in weak bias condition, vanishes. Instead, the three curves behave similarly. Each curve is composed of two pairs of strongly deformed two-level Fano line shapes with opposite sign of the Fano parameter. Resonances above and below $\epsilon_1 = -1$ are in phase respectively and out of phase mutually. This feature of conductance curves shows that the phases of resonances are no longer strongly altered by the level position ϵ_2 but ϵ_1 above or below $\epsilon_1 = -1$. In Fig. 5(d), with $\varphi = \pi$, the phases of four resonances are simultaneously changed by the RSO coupling, including the curve at $\epsilon_2 = -1$. Therefore, peaks and valleys in Fig. 5(a) are now

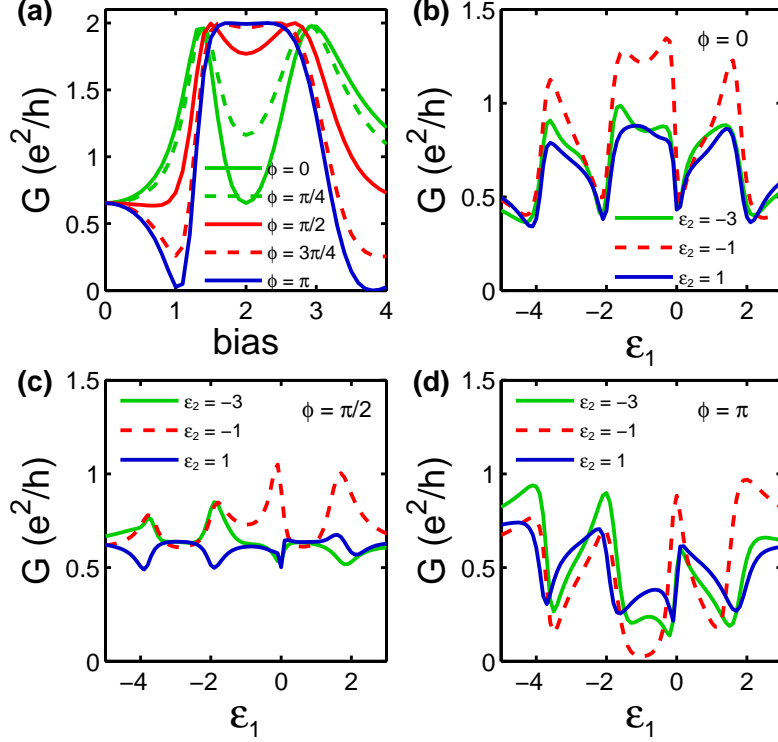


FIG. 5: (Color online) (a) Differential conductance at $\epsilon_1 = \epsilon_2 \equiv \epsilon = -1$ for $\varphi = 0, \pi/4, \pi/2, 3\pi/4, \pi$. Differential conductance for $\epsilon_2 = -3, -1, 1$ at (b) $\varphi = 0$, (c) $\varphi = \pi/2$, and (d) $\varphi = \pi$.

switched.

IV. SPIN POLARIZATION

In the absence of external magnetic field threading through the dots, a spin-unpolarized DQD is expected, with occupation numbers decreasing with increasing level position. An electric field established on semiconductor heterostructure serves as an effective magnetic field on moving electrons in 2DEG, and in consequence leads to a spin splitting. This spin splitting between up- and down-spin electrons combined with quantum interference can bring the spin-polarized occupation. In the preceding analysis we show that the spin accumulation on DQD can be induced in this device and depends on the variation in RSO coupling strength, meaning that the electron spin can be manipulated by simply tuning a gate voltage.

Figure 6(a) shows the electron occupation on the 2nd dot as a function of a common gate

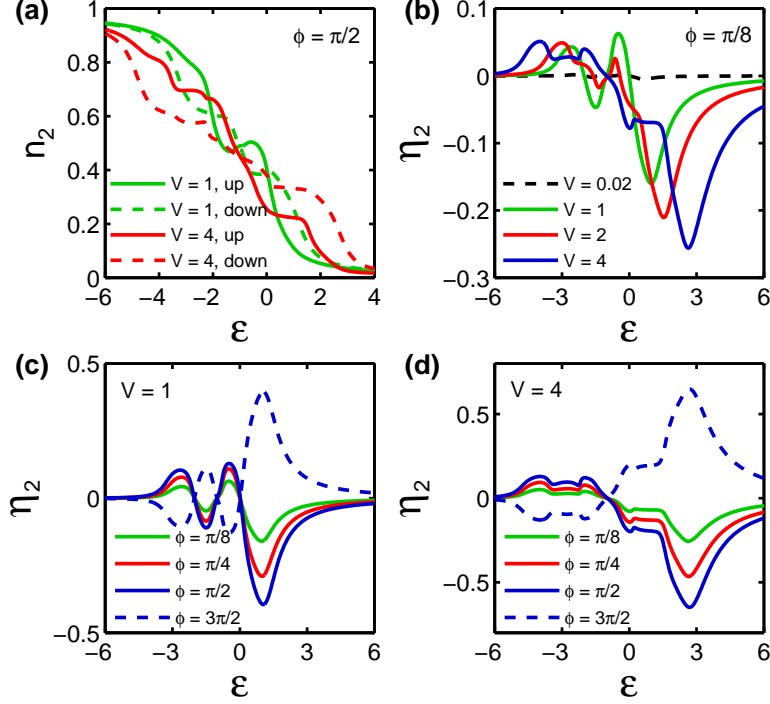


FIG. 6: (Color online) (a) Up- and down-spin electron occupation on the 2nd dot with $\epsilon_1 = \epsilon_2 \equiv \epsilon$ at $\varphi = \pi/2$. Green curves are for $V = 1$ and red curves are for $V = 4$. (b) Spin polarization at $\varphi = \pi/8$ for $V = 0.02, 1, 2, 4$. Spin polarization for $\varphi = \pi/8, \pi/4, \pi/2, 3\pi/2$ at (c) $V = 1$ and (d) $V = 4$.

voltage $\epsilon_1 = \epsilon_2 \equiv \epsilon$ at RSO coupling strength $\varphi = \pi/2$. In the presence of RSO interaction the spin degeneracy is lifted, and the dot is spin-polarized with spin accumulation $n_{2\uparrow} - n_{2\downarrow}$ changing with the level position. At bias $V = 4$, the curves for up and down spins intersect at $\epsilon = -1$. The spin accumulation on the left side of this point is positive while on the other side is negative. In addition to this crossing point, two more points around $\epsilon = 0$ and $\epsilon = -2$ in the curves at $V = 1$ are observed. By these well-separated curves for up and down electron spins, a spin-polarized dot is here verified. We then study the influence of tunable bias and RSO interaction on the SP, defined as $\eta_i \equiv (n_{i\uparrow} - n_{i\downarrow}) / (n_{i\uparrow} + n_{i\downarrow})$.

Let us first consider the situation, at fixed RSO coupling strength $\varphi = \pi/8$, with different values of bias from weak to strong condition, as shown in Fig. 6(b). SP on the DQD is tiny, $< 5\%$, when weak bias is applied to the device. As the value moves to strong bias region, the SP grows over 10% and obviously varies with ϵ . In the curves at $V = 1$ and $V = 2$,

there are three crossing points in negative ϵ region. We can clearly see that two crossing points, located at $\epsilon = 0, -2$ when $V = 1$, move toward each other as the bias increases. Subsequently they collide with the central one to disappear at about $V = 2.3$, leaving single crossing point for larger value of bias $V = 4$, for example. Thus, in strong bias condition, SP invariably changing sign at $\epsilon = -1$ is observed. This characteristic of SP meanwhile provides the possibility for the operation of spin flipping on the dot. In positive ϵ region a valley exists in each curve. This valley shifts to larger value of ϵ and becomes deeper with increasing bias. With such small RSO coupling strength, the maximum value of SP is found to be -25% . For larger value $\varphi = \pi/2$, the SP can even reach -65% at $V = 4$, as shown later in Fig. 6(d).

Now we discuss the behavior of induced SP altered by the RSO coupling strength. Figure 6(c) shows the SP, with $V = 1$, as a function of ϵ for $\varphi = \pi/8, \pi/4, \pi/2, 3\pi/2$. In negative ϵ region one can observe that the SP fluctuates about zero, which is consistent with the corresponding occupation in Fig. 6(a). With increase of RSO coupling the SP increases as well, with profile of the curve unchanged. The maximum values of the fluctuation and the valley go from 4% to 10% and from -16% to -40% , respectively. Once we flip φ with respect to π , from $\pi/2$ to $3\pi/2$, we can see clearly that the SP totally flips with respect to zero. Hence the peak and the valley are switched. In Grundler's experiment,²⁵ with a 2DEG on InAs-based heterostructure, the measured maximum value of Rashba parameter is $\alpha_R \approx 0.4 \text{ eV \AA}$. By this value of α_R , $\varphi = \pi/4$ corresponds to typical self-assembled dot size $L/2 \approx 20 \text{ nm}$, while φ can reach 5.67 with conventional gate-defined DQD size $L = 300 \text{ nm}$. Therefore, both the magnitude and the flip of SP, as observed here in Figs. 6(b) and (c), can be realized experimentally. Concerning the case $V = 4$, as shown in Fig. 6(d). Two characteristics of SP, i.e. increase and reversal with varied φ , exist similarly as the case $V = 1$ except that the fluctuations vanish and the overall values of SP are higher.

At last we address the relation between electron occupation on two dots. The difference of up spin, $\delta n \equiv n_2 - n_1$, as a function of ϵ is plotted at $\varphi = \pi/8, \pi/4, \pi/2$ and $V = 1, 2, 4$, as shown in Figs. 7(a) and (b), respectively. In both figures δn is highly symmetric with respect to $\epsilon = -1$. The increase of RSO coupling appears to suppress the difference. Increasing bias, moreover, shifts δn toward the negative and causes the peak splitting, which is ascribed to more Coulomb peaks entering the transport window.

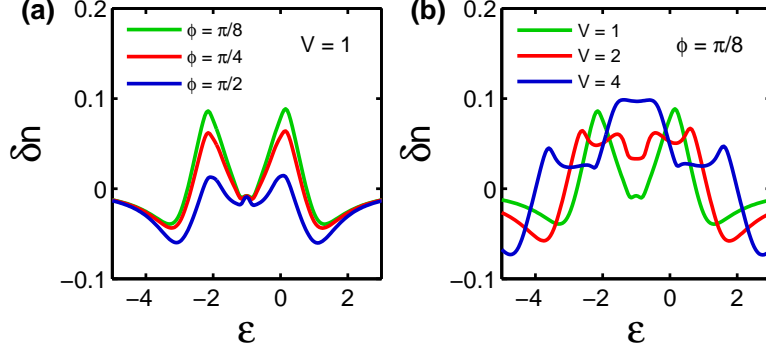


FIG. 7: (Color online) Occupation difference of up spin (a) at $V = 1$ for $\varphi = \pi/8, \pi/4, \pi/2$ and (b) at $\varphi = \pi/8$ for $V = 1, 2, 4$.

V. CONCLUSION

We have studied the quantum transport through a ring with embedded DQD, in which RSO interaction and on-site Coulomb repulsion are considered. Our analysis focuses on quantum interference and spin accumulation, with influence of both RSO coupling and nonequilibrium effect. For $V < 0.1U$, conductance in this linear response regime shows two pairs of Fano resonances. With gradual increase of $\varphi = 0$ to π , antiresonances are well resolved, because dot-lead matrix elements for up- and down-spin electrons are altered by the spin-dependent phase associated with spin precession on dots. Consequently both bonding and antibonding resonances are varied with phase difference π . For $V > 0.1U$, differential conductance noticeably changes with bias and RSO coupling strength. Such large bias window leads to more conductance peaks, when each molecular state is aligned with either of leads. However, the strength of resonances is notably suppressed due to the mixture of various kind of interference, arising from accessible excited states. In the study of transport through the tunable ϵ_1 , similar Fano line shapes in conductance for fixed $\epsilon_2 = -3, -1, 1$ show that the dependence of corresponding phases on ϵ_2 is strongly weakened. Instead, the dependence on ϵ_1 above or below $\epsilon_1 = -1$ is observed. Furthermore, with the help of a bridge channel, SP on serially coupled DQD can be achieved through the RSO interaction. We note that both of the increase of bias and RSO coupling strength can strengthen this SP. As $V < 2.3$, SP behaves similarly, with a fluctuation about zero for $\epsilon < 0$ and a deep valley for $\epsilon > 0$, except that the deeper valley shifts to higher energy position as bias increases.

As $V > 2.3$, the fluctuation is removed, leaving a substantial sign-changed point at $\epsilon = -1$. Meanwhile, SP can instantaneously flip once φ is tuned to cross π , which leads to a deep valley reversed to a high peak. Therefore, we have shown that the SP can be controlled to point along either up or down by simply switching the dot levels and the RSO coupling strength with respect to $\epsilon = -1$ and $\varphi = \pi$, respectively.

VI. ACKNOWLEDGMENTS

This work was supported by the Republic of China National Science Council under Grant No. 95-2112-M-002-044-MY3.

-
- ¹ H.-A. Engel and D. Loss, Phys. Rev. Lett. **93**, 136602 (2004).
 - ² Q.-F. Sun, X. C. Xie, and J. Wang, Phys. Rev. B **77**, 035327 (2008).
 - ³ D. Loss and D. P. DiVincenzo, Phys. Rev. A **57**, 120 (1998).
 - ⁴ R. López, D. Sánchez, and L. Serra, Phys. Rev. B **76**, 035307 (2007).
 - ⁵ V. N. Golovach, A. Khaetskii, and D. Loss, Phys. Rev. B **77**, 045328 (2008).
 - ⁶ Q.-F. Sun and X. C. Xie, Phys. Rev. B **73**, 235301 (2006).
 - ⁷ A. M. Lobos and A. A. Aligia, Phys. Rev. Lett. **100**, 016803 (2008).
 - ⁸ F. M. Alves, C. Trallero-Giner, V. Lopez-Richard, and G. E. Marques, Phys. Rev. B **77**, 035434 (2008).
 - ⁹ J. Nitta, T. Akazaki, H. Takayanagi, and T. Enoki, Phys. Rev. Lett. **78**, 1335 (1997).
 - ¹⁰ D. Rohrlich, O. Zarchin, M. Heiblum, D. Mahalu, and V. Umansky, Phys. Rev. Lett. **98**, 096803 (2007).
 - ¹¹ A. Yacoby, M. Heiblum, D. Mahalu, and H. Shtrikman, Phys. Rev. Lett. **74**, 4047 (1995).
 - ¹² M. Sigrist, T. Ihn, K. Ensslin, M. Reinwald, and W. Wegscheider, Phys. Rev. Lett. **98**, 036805 (2007).
 - ¹³ J. Gores, D. Goldhaber-Gordon, S. Heemeyer, M. A. Kastner, H. Shtrikman, D. Mahalu, and U. Meirav, Phys. Rev. B **62**, 2188 (2000).
 - ¹⁴ K. Kobayashi, H. Aikawa, S. Katsumoto, and Y. Iye, Phys. Rev. Lett. **88**, 256806 (2002).

- ¹⁵ A. C. Johnson, C. M. Marcus, M. P. Hanson, and A. C. Gossard, Phys. Rev. Lett. **93**, 106803 (2004).
- ¹⁶ U. Fano, Phys. Rev. **124**, 1866 (1961).
- ¹⁷ Y. S. Joe, A. M. Satanin, and G. Klimeck, Phys. Rev. B **72**, 115310 (2005).
- ¹⁸ A. A. Clerk, X. Waintal, and P. W. Brouwer, Phys. Rev. Lett. **86**, 4636 (2001).
- ¹⁹ L. V. Keldysh, Sov. Phys. JETP **20**, 1018 (1965).
- ²⁰ A. Fuhrer, P. Brusheim, T. Ihn, M. Sigrist, K. Ensslin, W. Wegscheider, and M. Bichler, Phys. Rev. B **73**, 205326 (2006).
- ²¹ Q.-F. Sun, J. Wang, and H. Guo, Phys. Rev. B **71**, 165310 (2005).
- ²² Y. Meir and N. S. Wingreen, Phys. Rev. Lett. **68**, 2512 (1992).
- ²³ A. Silva, Y. Oreg, and Y. Gefen, Phys. Rev. B **66**, 195316 (2002).
- ²⁴ W.-R. Lee, J. U. Kim, and H.-S. Sim, Phys. Rev. B **77**, 033305 (2008).
- ²⁵ D. Grundler, Phys. Rev. Lett. **84**, 6074 (2000).